The TRPV2 channel mediates Ca^{2+} influx and the Δ9-THC-dependent decrease in osmotic fragility in red blood cells

Water and ionic homeostasis of red blood cells (RBC) is regulated by various active and passive transport mechanisms in the RBC membrane, including channels like aquaporins,[1] the mechanically activated non-selective cation channel Piezo1[2] and the Ca^{2+}-activated potassium channel KCa3.1.[3] The human genome contains 27 genes that code for transient receptor potential (TRP) channels. The only TRP channel protein that has been detected in circulating mouse RBC is TRPC6,[4] which might be associated with basal Ca^{2+} leakage and stress-stimulated Ca^{2+} entry.[4] TRPC2 and TRPC3 are expressed by murine erythroid precursors and splenic erythroblasts, and in these cells, erythropoietin stimulates an increase in intracellular calcium concentration via TRPC2 and TRPC3.[5] In this study we identified the TRP vanilloid (TRPV) 2 channel protein in mouse and human RBC by specific antibodies and mass spectrometry. TRPV2-dependent currents and Ca^{2+} entry were activated by the TRPV2 agonists cannabidiol (CBD) and Δ9-tetrahydrocannabinol (Δ9-THC)[6] resulting in a left-shift of the hypotonicity-dependent hemolysis curve. This effect was reversed in the presence of the KCa3.1 inhibitor TRAM-34, whereas the knockout of *Trpv2* right-shifted the hemolysis curve to higher tonicities.

We separated mouse RBC from other blood cells by centrifugation and analyzed protein lysates by nanoflow liquid chromatography tandem mass spectrometry (nano-LC-MS/MS). The identified proteins included TRPV2 (*Online Supplementary Figure S1A*). To enrich the TRPV2 protein we generated an antibody which recognizes the TRPV2 protein in RBC from wild-type (WT) animals but not in RBC from *Trpv2* gene-deficient (KO) mice (Figure 1A). As an additional control, we used anti-TRPC6 antibody and identified TRPC6 in RBC (Figure 1B). Total eluates of anti-mTRPV2 affinity purifications from RBC membranes of WT mice were analyzed by nano-LC-MS/MS, which retrieved peptides covering 54% of the accessible TRPV2 primary sequence (*Online Supplementary Figure S1B*).

To obtain a more comprehensive protein profile, we lysed WT and *Trpv2*-KO RBC, extracted the proteins, and measured the resulting tryptic peptides by nano-LC-MS/MS. A total of 1,450 proteins were identified (*Online Supplementary Figure S1E*), with TRPV2 present in all WT samples. Eighty-seven of the identified proteins were detected exclusively or with more than a 2-fold increase in WT RBC, while 13 proteins were detected with more than a 2-fold increase in *Trpv2*-KO RBC (Figure 1C, *Online Supplementary Figure S1F*) by semiquantitative exponentially modified protein abundance index (emPAI) analysis. Next, we evaluated the frequency of the identified proteins by spectral counting and normalized the data to band 3 (Figure 1D). TRPV2 ranked at position 560, about 0.4% of band 3, 50% and 84% less than ferroportin and Piezo1, respectively. In addition to TRPV2 and Piezo1, other channels such as aquaporin1 and transmembrane channel like 8 (*Online Supplementary Figure S1D*) were identified. The KCa3.1 protein, on the other hand, seemed to be much less abundant, as we could identify only one KCa3.1 peptide in our experiments, which was below the threshold for unambiguous protein identification.

According to the proteomic profiling, Piezo1 and aquaporin1 proteins were present in equal amounts in murine RBC from *Trpv2*-KO and WT animals. In contrast, several proteins that affect ion and fluid homeostasis were significantly less abundant in *Trpv2*-KO RBC, including the STE20-like- and the WNK1-serine/threonine protein kinases SLK (in humans also dubbed SPAK) and WNK1 (Figure 1C). Both kinases regulate the Na^+-K^+-Cl^- symporter NKCC1 present in the erythrocyte membrane, resulting in the flux of NaCl and KCl into the cell with subsequent rehydration.[7] This mechanism would be attenuated in *Trpv2*-KO RBC with decreased WNK1, similar to renal cells that are also equipped with NKCC1 and WNK1 and in which WNK1 is inhibited under hypotonic conditions. Likewise, the significantly reduced amount of the casein kinase II (CKII)-α subunit (CSK21) in *Trpv2*-KO RBC (Figure 1C) could be part of mechanisms that compensate for the absence of TRPV2, as pharmacological inhibition of CKII-α causes shrinkage of RBC.[8]

Hematologic parameters from blood of *Trpv2*-KO and WT animals (Figure 1E), were not significantly different. However, when RBC were exposed to hypotonic solutions, keeping extracellular [Ca^{2+}] at 76 μM, hemolysis of *Trpv2*-KO RBC occurred at higher tonicity (Figure 1F). The relative tonicity at half maximal lysis (C_{50}) (Figure 1G) was 49.19±0.62 (WT, n=5) and 53.7±0.68 (*Trpv2*-KO, n=5; $P<0.0001$).

To isolate TRPV2 currents from murine RBC we applied the non-specific TRPV2 agonist 2-APB. Inward and outward currents with the outwardly rectifying current-voltage (IV) relationship typical of TRPV2 currents were recorded by whole cell patch-clamping (Figure 2A, B) or by a miniaturized patch system (Figure 2C, D). A fraction of these 2-APB-induced currents was blocked by ruthenium red. Similar, but much larger currents were recorded from COS-7 cells, which overexpress the murine *Trpv2* cDNA (*Online Supplementary Figure S2E*). Upon application of 2-APB, cytoplasmic [Ca^{2+}] increased in WT RBC (*Online Supplementary Figure S2A*). The Ca^{2+} increase was blocked in the presence of ruthenium red but could also be induced in *Trpv2*-KO RBC (*Online Supplementary Figure S2B-D*). 2-APB blocks TRPC6 and KCa3.1 present in RBC and acts on additional targets.[9] Thereby it may affect the RBC membrane potential and Ca^{2+}-signaling pathways independently of TRPV2 during monitoring cytoplasmic Ca^{2+}. As shown in COS-7 cells (*Online Supplementary Figures S2E-I* and *S3A*), which do not endogenously express TRPC6 or KCa3.1, the 2-APB-induced increase in cytosolic Ca^{2+} and plasma membrane currents required the presence of overexpressed mouse or human TRPV2. We therefore applied the more specific TRPV2 agonist Δ9-THC, which elicited Ca^{2+} influx in WT RBC; this influx was significantly reduced in *Trpv2*-KO RBC (Figure 2E, F) indicating that part of the Ca^{2+} increase was mediated by TRPV2. The antagonists of the G protein-coupled cannabinoid receptors type 1 (CB1) and type 2 (CB2), AM251 (AM) and JTE907 (JTE), had no effect on the Δ9-THC-elicited Ca^{2+}-response in WT RBC (Figure 2G, H), demonstrating that TRPV2 mediates a significant fraction of THC-elicited Ca^{2+} influx and that the action of THC on TRPV2 is direct, and not mediated by CB1 or CB2 receptors.

The primary sequences of human and mouse TRPV2 are 80.4% identical, but the antibody against mTRPV2 does not recognize the hTRPV2 protein. We therefore generated an antibody that recognizes the hTRPV2 protein by western blot (Figure 3A). Next, total eluates of anti-hTRPV2 affinity purifications from RBC membranes were analyzed by nano-LC-MS/MS that retrieved peptides covering 54.8% of the hTRPV2 primary sequence (*Online Supplementary Figure S1G*). In similar experiments but with an antibody for hTRPC6, TRPC6 was not detectable in human RBC by either western blot or nano-LC-MS/MS.

The cannabinoid TRPV2 agonists CBD and Δ9-THC

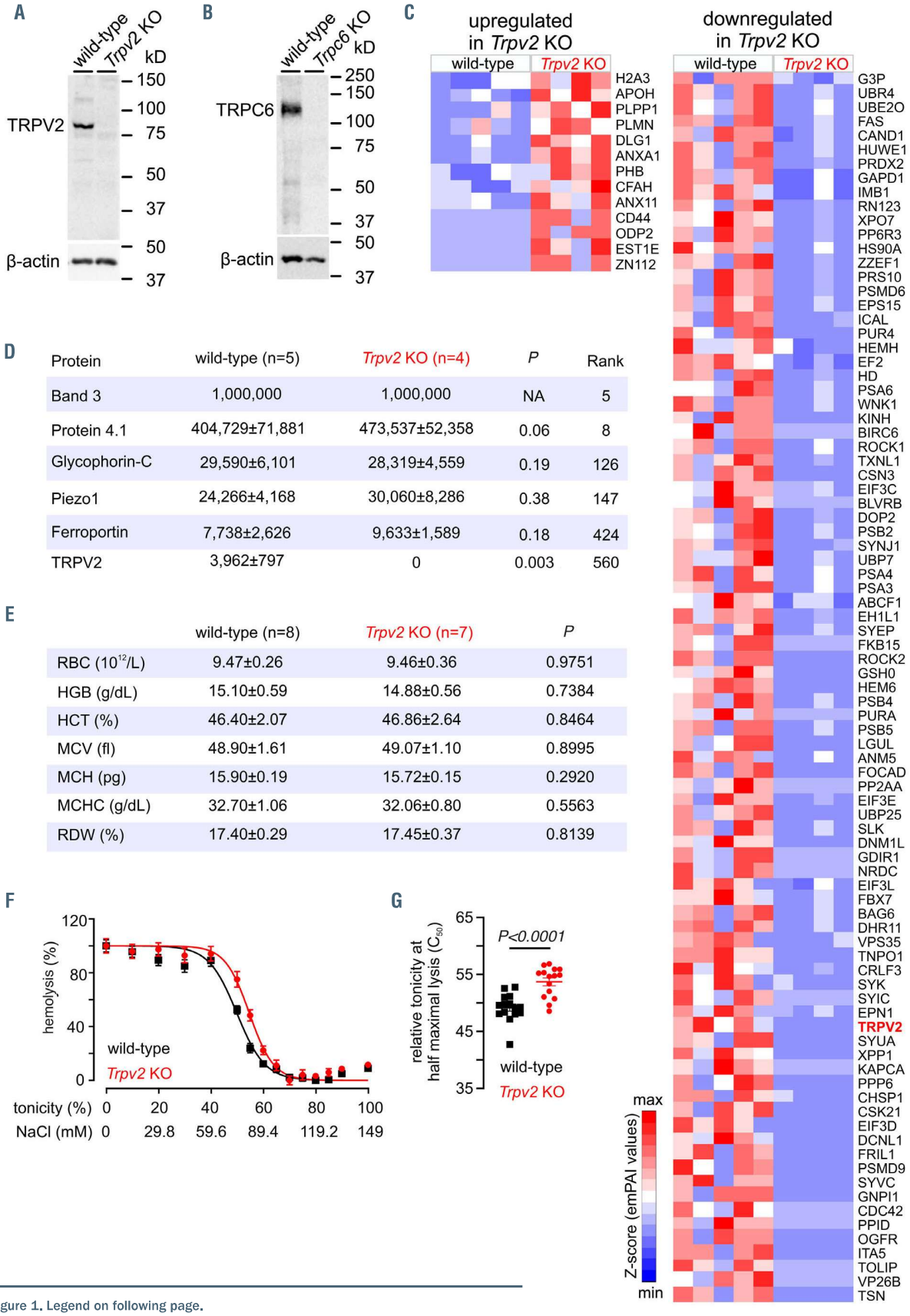

D

Protein	wild-type (n=5)	*Trpv2* KO (n=4)	*P*	Rank
Band 3	1,000,000	1,000,000	NA	5
Protein 4.1	404,729±71,881	473,537±52,358	0.06	8
Glycophorin-C	29,590±6,101	28,319±4,559	0.19	126
Piezo1	24,266±4,168	30,060±8,286	0.38	147
Ferroportin	7,738±2,626	9,633±1,589	0.18	424
TRPV2	3,962±797	0	0.003	560

E

	wild-type (n=8)	*Trpv2* KO (n=7)	*P*
RBC (10^{12}/L)	9.47±0.26	9.46±0.36	0.9751
HGB (g/dL)	15.10±0.59	14.88±0.56	0.7384
HCT (%)	46.40±2.07	46.86±2.64	0.8464
MCV (fl)	48.90±1.61	49.07±1.10	0.8995
MCH (pg)	15.90±0.19	15.72±0.15	0.2920
MCHC (g/dL)	32.70±1.06	32.06±0.80	0.5563
RDW (%)	17.40±0.29	17.45±0.37	0.8139

Figure 1. Legend on following page.

Figure 1. TRPV2 protein in mouse red blood cells. (A, B) Western blot of wild-type, *Trpv2* knockout (KO) (A) and *Trpc6* KO (B) red blood cell (RBC) proteins, using antibodies against mouse TRPV2, TRPC6 and β-actin. (C) Semi-quantitative analysis of differentially expressed proteins identified by mass spectrometry in wild-type and *Trpv2* KO RBC lysates. Up- and down-regulated proteins were identified based on at least 2-fold changes with a *P*-value <0.05, calculated by an unpaired two-tailed Student *t* test. The heatmap shows the Z-scores of the exponentially modified protein abundance index (emPAI) values of mass spectrometry measurements of five independent wild-type and four independent *Trpv2* KO samples. (D) Relative abundance of the TRPV2 protein compared to that of the 1,450 proteins identified in mouse erythrocyte membrane fractions. Rank represents the order of the identified protein obtained by spectral counting with the *P*-value calculated by an unpaired Student *t* test. NA, not applicable. (E) Hematologic parameters of the blood from wild-type and *Trpv2* KO. RBC: red blood cell; HGB: hemoglobin; HCT: hematocrit; MCV: mean corpuscular volume; MCH: mean corpuscular hemoglobin; MCHC: mean corpuscular hemoglobin concentration; RDW: red cell distribution width with *P*-value calculated by an unpaired two-tailed Student *t* test. (F) Hemolysis (%) of RBC collected from wild-type (black) and *Trpv2* KO mice (red) in buffer A (149 mM NaCl, 2 mM $CaCl_2$, 4 mM KCl, 2 mM HEPES, pH7.4), diluted 26-fold in buffer B (0-149 mM NaCl, 2 mM HEPES, pH 7.4) as indicated; extracellular [Ca^{2+}] was kept at ~76 μM. (G) Tonicity at which 50% lysis occurred (C_{50}), calculated by sigmoidal fitting from experiments in (F). Single values and mean ± standard error of mean from five independent experiments performed in triplicate are shown with the *P*-value calculated by an unpaired two-tailed Student *t* test.

elicited Ca^{2+} influx in human RBC (Figure 3B-D). Inward and outward currents with the outward rectifying IV relation were obtained by patch clamp recordings from human RBC after application of Δ9-THC (Figure 3E-G). Although the currents obtained from human RBC have a small amplitude, their IV match the TRPV2 current signature obtained from COS-7 overexpressing human TRPV2 cDNA upon application of Δ9-THC or CBD (*Online Supplementary Figure S3B, C*).

Assessment by confocal microscopy revealed that 95.3±2.4% of the human RBC had a biconcave disc-shaped form. Adding CBD or Δ9-THC shifted the morphology of these biconcave discocytes to concave RBC, the stomatocytes, which in the presence of CBD and Δ9-THC make up 92.7±1.3% (CBD) and 66.3±17.1% (THC) of the total RBC, the remaining cells being discocytes and more spherical-shaped spherocytes (Figure 3H, I). The TRPV2 agonist-induced shape change of the RBC was maintained in the presence of the CB1 and CB2 antagonists (*Online Supplementary Figure S3D, E*), indicating that the major fraction of the cannabinoids' effect on RBC morphology is mediated by TRPV2. After addition of Δ9-THC, human RBC showed reduced osmotic fragility, as demonstrated by the left-shifted hemolysis curve in response to the hypotonicity challenge, independently of whether cannabinoid receptor antagonists were absent or present (Figure 3J, K). Similarly, but to a lesser extent, Δ9-THC shifts the C_{50} value after treating WT murine RBC to lower tonicities (C_{50}, in the absence, 49.05±1.53, and in the presence of Δ9-THC, 46.08±1.55). This effect was reversed by pretreatment with the KCa3.1 antagonist TRAM-34, in the presence of 76 μM (*Online Supplementary Figure S3F, G*)

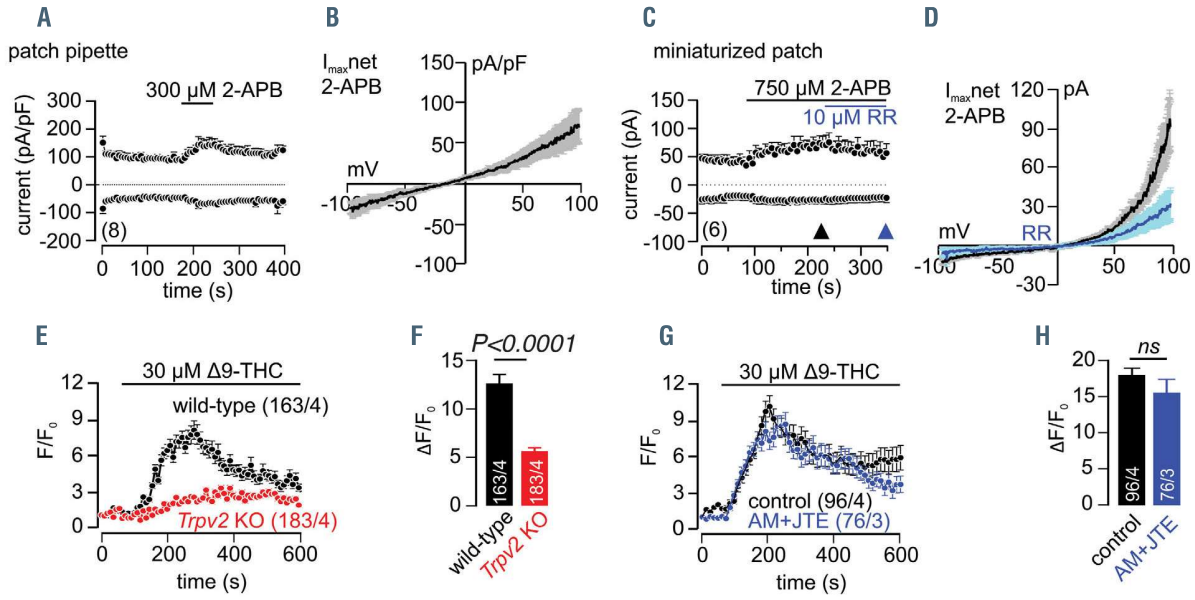

Figure 2. TRPV2 function in mouse red blood cells. (A-D) In- and outward currents at -80 and +80 mV shown as mean ± standard error of mean (SEM), recorded from mouse red blood cells (RBC) using a patch pipette (A) or a miniaturized patch clamp system (port-a-patch) (C) plotted *versus* time (number of cells in brackets). TRPV2 currents were activated by the application of 2-APB (black line) in the absence and presence of 10 μM ruthenium red (RR, blue line) with the corresponding current-voltage relationships (IV) at the peak net currents (I_{max} net), shown as mean ± SEM in (B) and (D). Patch pipette resistances were 10 - 15 MΩ when filled with standard internal solution (in mM): 120 Cs-glutamate, 8 NaCl, 1 $MgCl_2$, 10 HEPES, 10 1,2-bis(2-aminophenoxy)ethane-N,N,N',N'-tetraacetic acid tetracesium salt (Cs-BAPTA), 3.1 $CaCl_2$ (100 nM free Ca^{2+}, calculated with WebMaxC), pH7.2 with CsOH. Standard external solution contained (in mM): 140 NaCl, 2 $MgCl_2$, 1 $CaCl_2$, 10 HEPES, 10 glucose, pH 7.2 with NaOH. For experiments with the miniaturized patch system, the intracellular solution contained (in mM): 60 Cs-methansulfonate, 8 NaCl, 1 $MgCl_2$, 3.1 $CaCl_2$, 60 CsF, 10 HEPES, 10 BAPTA (100 nM free Ca^{2+}, calculated with WebMaxC), 10 glucose, pH 7.2 with CsOH and the extracellular solution contained (in mM): 140 NaCl, 2 $MgCl_2$, 1.35 $CaCl_2$, 10 HEPES, 10 glucose, pH 7.2 with NaOH. (E, G) Mean Fluo-4 fluorescence (F/F_0) traces showing changes in the cytosolic [Ca^{2+}] of RBC isolated from wild-type (black) and *Trpv2* KO mice (red) in the absence (E) and presence (G, blue) of the CB1/CB2-receptor antagonists AM251 and JTE907 (100 nM each), challenged by the application of 30 μM Δ9-tetrahydrocannabinol (Δ9-THC, line). Ca^{2+}-imaging measurements were performed in the presence of a Tyrode solution (in mM): 135 NaCl, 5.4 KCl, 1 $MgCl_2$, 10 HEPES, 10 glucose, and 1.8 $CaCl_2$, pH 7.35; RBC were loaded with 5 μM Fluo-4 and the fluorescence was excited at 488 nm every 3 seconds with the emitted fluorescence detected at >515 nm. (F, H) Summary of peak amplitudes from (E) and (G) shown as mean ± SEM with *P*-values calculated by the unpaired two-tailed Student *t* test (ns, not significant). Numbers of measured cells (x) within (y) independent experiments are indicated in brackets and bars.

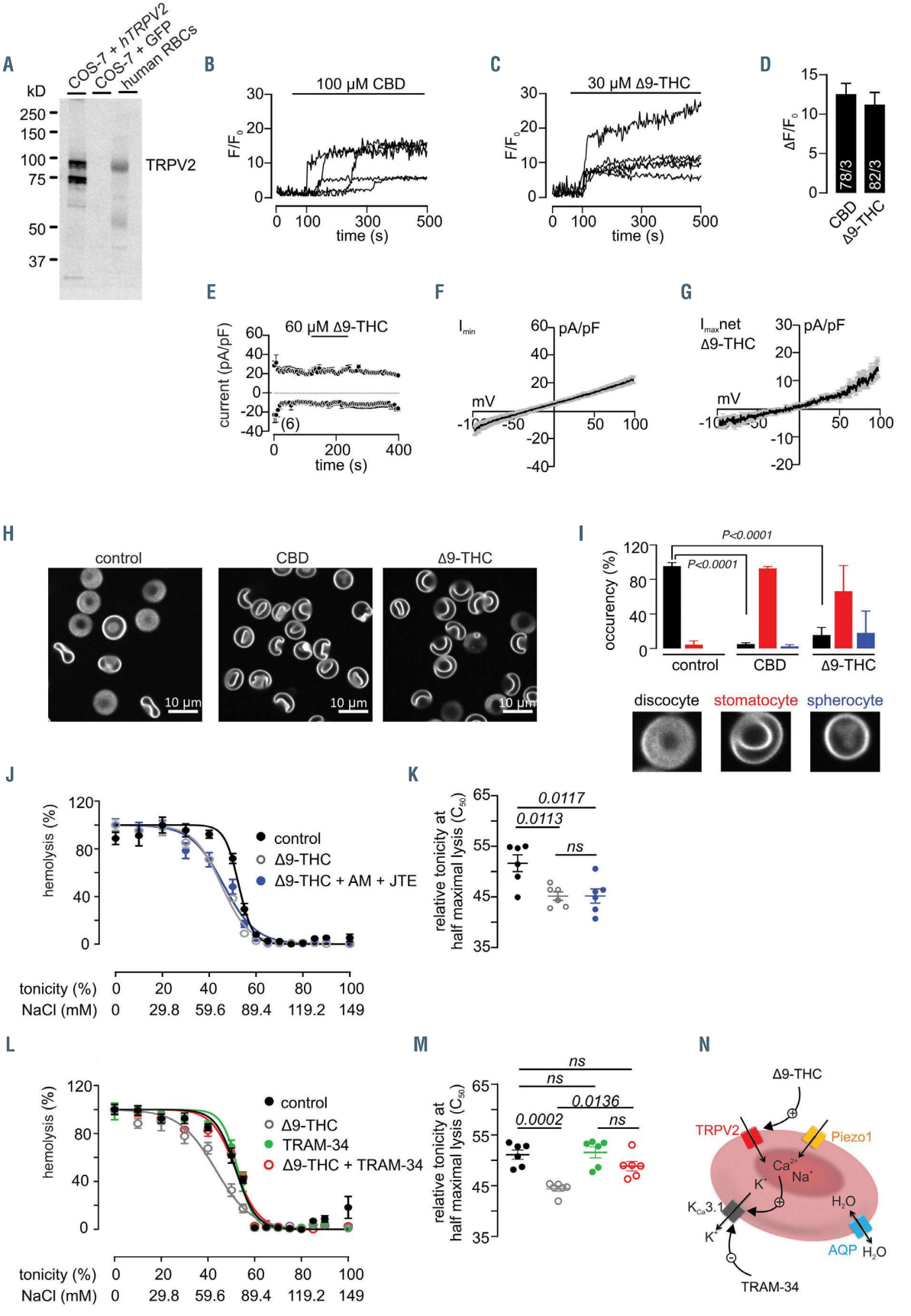

Figure 3. Legend on following page.

Figure 3. TRPV2 protein and function in human red blood cells. (A) Western blot of protein lysates of COS-7 cells transfected with human *TRPV2* cDNA, the cDNA of green fluorescent protein (GFP) as a control, and human red blood cells (RBC) using anti-human TRPV2. (B, C) Representative traces of cytosolic Ca^{2+} changes, detected as Fluo-4 fluorescence (F/F_0), in human RBC challenged by the application of 100 μM cannabidiol (CBD) (B) or 30 μM Δ9-tetrahydrocannabinol (Δ9-THC) (C). (D) Summary of the peak amplitudes in (B) and (C) as mean ± standard error of mean (SEM) (78 and 82 cells measured in 3 independent experiments each). (E) In- and outward currents at -80 and +80 mV in the absence and presence of Δ9-THC (black line) recorded from human RBC and plotted versus time. The corresponding current-voltage relationships (IV) of the basic current (I_{min}) and the peak net current in Δ9-THC (I_{max} net) are depicted in (F) and (G). Data are shown as mean ± SEM (number of cells indicated in brackets). (H) Confocal microscopic images of human RBC not treated (control, left) or treated with 100 μM cannabidiol (CBD, middle) or 30 μM Δ9-THC (right). (I) Bar graphs showing the percentage of discocytes (black), stomatocytes (red) and spherocytes (blue) as mean ± SEM, from three independent healthy donors, treated as in (H), with *P*-values calculated by one-way analysis of variance (ANOVA), followed by the Bonferroni multiple comparison. The classification was done with 3-D stacks of confocal images. (J) Hemolysis (%) of human RBC treated with the vehicle (control, black), 30 μM Δ9-THC (gray open circle) or 30 μM Δ9-THC in the presence of 100 nM CB1- and CB2-receptor antagonists AM251 and JTE907 (Δ9-THC + AM + JTE, blue) plotted *versus* the extracellular NaCl concentration (mM) and respective tonicity (%), with extracellular $[Ca^{2+}]$ kept at 76 μM as described in Figure 1F. (K) Tonicity at which 50% lysis occurred (C_{50}), calculated by sigmoidal fitting of the individual experiments in (J). (L) Hemolysis (%) of human RBC in buffer A (149 mM NaCl, 2 mM $CaCl_2$, 4 mM KCl, 2 mM HEPES, pH 7.4), treated with vehicle (control, black), 30 μM Δ9-THC (gray open circle), 2 μM TRAM-34 (green) or 30 μM Δ9-THC plus TRAM-34 (red) for 30 min, after 26-fold dilution in buffer B (0-149 mM NaCl, 2 mM $CaCl_2$, 4 mM KCl, 2 mM HEPES, pH 7.4); extracellular $[Ca^{2+}]$ was kept at 2 mM. (M) Tonicity at which 50% lysis occurred (C_{50}), calculated by sigmoidal fitting of the individual experiments in (L). Data in (K) and (M) are shown as means ± SEM from two independent experiments performed in triplicate with the *P*-value calculated by one-way ANOVA, followed by the Bonferroni multiple comparison. (N) Working model for how TRPV2, activated by Δ9-THC, modulates the TRAM-34 sensitive KCa3.1 activity in a human RBC. Note that TRPC6 was not detectable in human RBC.

or 2 mM extracellular Ca^{2+} (Figure 3L, M). The data indicate that TRPV2, like Piezo1 and, maybe TRPC6, enables an influx of cations including Ca^{2+}. The increase of intracellular Ca^{2+} by TRPV2 activates KCa3.1 which allows K^+ efflux, resulting in the shift of the hemolysis curve. This shift does not occur in the presence of the KCa3.1 antagonist TRAM-34 (Figure 3L-N).

Stabilization of the RBC membrane against hypotonic hemolysis by Δ9-THC and CBD has been described[10] and it has been shown that in the presence of Δ9-THC at concentrations of >15 μM almost all RBC assume a stomatocyte-like concave shape.[11] Some of those results were attributed to interactions between the hydrophobic, naturally occurring cannabinoids and the membrane lipids of the RBC. However, membrane partitioning experiments, electron spin resonance spectrometry and experiments with artificial liposomes of different compositions which were tested for the release of trapped markers in the presence of Δ9-THC, suggested additional mechanisms.[12-14]

The data described in our study point to TRPV2 being a specific molecular target for Δ9-THC and CBD in RBC. Activation of the TRPV2 channel by the compounds present in the *Cannabis sativa* plant makes RBC more resistant to lysis in response to hypotonic solutions. Whether our data explain why hemp products have been used in folk medicine to treat malaria since ancient times[15] needs to be shown by further studies.

Anouar Belkacemi,[1] Claudia Fecher-Trost,[1] René Tinschert,[1] Daniel Flormann,[2] Mahsa Malihpour,[1] Christian Wagner,[2,3] Markus R. Meyer,[1] Andreas Beck[1] and Veit Flockerzi[1]

[1]Experimentelle und Klinische Pharmakologie und Toxikologie und Präklinisches Zentrum für Molekulare Signalverarbeitung (PZMS), Universität des Saarlandes, Homburg, Germany; [2]Experimentalphysik, Universität des Saarlandes, Saarbrücken, Germany and [3]University of Luxembourg, Physics and Materials Science Research Unit, Esch-sur-Alzette, Luxembourg

Correspondence: VEIT FLOCKERZI - veit.flockerzi@uks.eu

doi:10.3324/haematol.2020.274951

Received: October 26, 2020.

Accepted: February 8, 2021.

Pre-published: February 18, 2021.

Disclosures: no conflicts of interest to disclose.

Contributions: ABelkacemi, CFT, RT, DF, MM, and ABeck performed experiments, ABelkacemi, CFT, DF, ABeck and VF analyzed data. MRM provided reagents. ABelkacemi, ABeck and VF conceived and supervised the study. CFT, ABeck, CW and MRM edited the manuscript. ABelkacemi and VF wrote the manuscript.

Acknowledgments: we thank Dr. Petra Weissgerber and the Transgene Unit of the SPF animal facility (project P2 of SFB 894) of the Medical Faculty, Homburg, for taking care of the mice; Christine Wesely, Martin Simon-Thomas, Oliver Glaser and Armin Weber for excellent technical assistance; Prof. Dr. Michael J. Caterina, the Johns Hopkins University (Baltimore) and the University of California San Francisco (UCSF), for providing the Trpv2 KO mouse strain.

Funding: the study was funded by the Deutsche Forschungsgemeinschaft (DFG) Collaborative Research Center 894 Project A3 (to ABelkacemi, VF) and A14 (to ABeck, VF) and FE 629/2-1 (to CFT).

References

1. Agre P, Preston GM, Smith BL, et al. Aquaporin CHIP: the archetypal molecular water channel. Am J Physiol. 1993;265(4 Pt 2):F463-476.
2. Cahalan SM, Lukacs V, Ranade SS, Chien S, Bandell M, Patapoutian A. Piezo1 links mechanical forces to red blood cell volume. Elife. 2015;4:e07370.
3. Maher AD, Kuchel PW. The Gardos channel: a review of the Ca^{2+}-activated K^+ channel in human erythrocytes. Int J Biochem Cell Biol. 2003;35(8):1182-1197.
4. Foller M, Kasinathan RS, Koka S, et al. TRPC6 contributes to the Ca^{2+} leak of human erythrocytes. Cell Physiol Biochem. 2008;21(1-3):183-192.
5. Hirschler-Laszkiewicz I, Zhang W, Keefer K, et al. Trpc2 depletion protects red blood cells from oxidative stress-induced hemolysis. Exp Hematol. 2012;40(1):71-83.
6. Pumroy RA, Samanta A, Liu Y, et al. Molecular mechanism of TRPV2 channel modulation by cannabidiol. Elife. 2019;8:e48792.
7. Zheng S, Krump NA, McKenna MM, et al. Regulation of erythrocyte $Na^+/K^+/2Cl^-$ cotransport by an oxygen-switched kinase cascade. J Biol Chem. 2019;294(7):2519-2528.
8. Kostova EB, Beuger BM, Klei TR, et al. Identification of signalling cascades involved in red blood cell shrinkage and vesiculation. Biosci Rep. 2015;35(2):e00187.
9. Hermosura MC, Monteilh-Zoller MK, Scharenberg AM, Penner R, Fleig A. Dissociation of the store-operated calcium current I(CRAC) and the Mg-nucleotide-regulated metal ion current MagNuM. J Physiol. 2002;539(Pt 2):445-458.
10. Chari-Bitron A. Stabilization of rat erythrocyte membrane by 1 - tetrahydrocannabinol. Life Sci II. 1971;10(22):1273-1279.
11. Chari-Bitron A, Shahar A. Changes in rat erythrocyte membrane induced by delta 1-tetrahydrocannabinol, scanning electron microscope study. Experientia. 1979;35(3):365-366.
12. Alhanaty E, Livne A. Osmotic fragility of liposomes as affected by antihelmolytic compounds. Biochim Biophys Acta. 1974;339(1):146-155.
13. Laurent B, Roy PE. Alteration of membrane integrity by delta1-tetrahydrocannabinol. Int J Clin Pharmacol Biopharm. 1975;12(1-2):261-266.
14. Leuschner JT, Wing DR, Harvey DJ, et al. The partitioning of delta 1-tetrahydrocannabinol into erythrocyte membranes in vivo and its effect on membrane fluidity. Experientia. 1984;40(8):866-868.
15. Touw M. The religious and medicinal uses of Cannabis in China, India and Tibet. J Psychoactive Drugs. 1981;13(1):23-34.